GEOPHYSICS, VOL. 85, NO. 4 (JULY-AUGUST 2020); P. B119–B131, 10 FIGS., 1 TABLE.
10.1190/GEO2019-0272.1

Case History

Using an airborne electromagnetic method to map saltwater intrusion in the northern Salinas Valley, California

Ian Gottschalk[1], Rosemary Knight[1], Theodore Asch[2], Jared Abraham[2], and James Cannia[2]

ABSTRACT

Saltwater intrusion can pose a serious threat to groundwater quality in coastal regions. Estimating the extent of saltwater intrusion is vital for groundwater managers to plan appropriate mitigation strategies. The airborne electromagnetic (AEM) method is commonly used to evaluate groundwater resources, but it is challenging to apply in coastal environments because the low resistivity of saltwater-saturated aquifers attenuates the electromagnetic signal quickly and the relationship between electrical resistivity and pore water salinity is complex. However, if successful, the AEM method can supply information to address questions of critical importance in coastal regions. We investigated the extent of, and controls on, saltwater intrusion using the AEM method in the northern Salinas Valley, CA, USA. We collected 635 line-km of AEM data in the study area, the inversion results of which produced estimates of the electrical resistivity of the subsurface, reaching depths of between 50 and approximately 200 m below the ground surface. We have developed a relationship between the AEM electrical resistivity model and groundwater salinity, calibrated from borehole geophysical and water quality measurements, which allowed us to generate images revealing the distribution of saltwater and fresher groundwater in the study area. This fresher groundwater (defined as "a source of drinking water") was successfully mapped out in the unconfined aquifer (the Dune Sand Aquifer) and the uppermost confined aquifer (the 180-Foot Aquifer) in the study area, illustrating a groundwater recharge process that helps mitigate saltwater intrusion in the 180-Foot Aquifer. Deep, low-resistivity bodies also were mapped, indicating regions where saltwater likely is migrating vertically from the 180-Foot Aquifer into the lower confined aquifer (the 400-Foot Aquifer). The findings from this case study demonstrate the value of acquiring AEM data for investigating the distribution of salinity in coastal aquifers impacted by saltwater intrusion.

INTRODUCTION

In coastal areas, freshwater and saltwater interact in the process of saltwater intrusion, where marine saltwater migrates into terrestrial aquifers. A freshwater-saltwater interface is established according to the pressure distribution in the aquifer, and the position of the freshwater-saltwater interface can vary with pressure changes in the aquifer. Such pressure changes often occur in heavily pumped aquifers, in which a decrease in aquifer pressure from groundwater extraction draws saltwater farther inland. Understanding the distribution of salinity within the aquifer system is essential for evaluating the current state of groundwater resources and also for assessing the potential impact of any proposed activity affecting the groundwater in the area. The aim of this case history was to map out regions of the subsurface containing saltwater and fresher water in the northern Salinas Valley, California, USA, using an airborne electromagnetic (AEM) method.

Manuscript received by the Editor 29 April 2019; revised manuscript received 26 February 2020; published ahead of production 5 June 2020; published online 15 June 2020.
[1]Stanford University, Geophysics Department, 397 Panama Mall, 3rd Floor, Stanford, California 94305, USA. E-mail: ianpg@stanford.edu (corresponding author); rknight@stanford.edu.
[2]Aqua Geo Frameworks LLC, 130360 County Road D, Mitchell, Nebraska 69357, USA. E-mail: tasch@aquageoframeworks.com; jabraham@aquageoframeworks.com; jcannia@aquageoframeworks.com.

Saltwater intrusion significantly affects the quality of groundwater in the northern Salinas Valley. Figure 1 shows the specific study area. The extent of saltwater intrusion in the region is mapped by the Monterey County Water Resources Agency (MCWRA) using information from wells provided to the public as a map of chloride contours, indicating where a chloride concentration of has been encountered in each of the two uppermost confined aquifers in the region, named the 180-Foot Aquifer and the 400-Foot Aquifer. (The names indicate the approximate depth below the ground surface to the aquifer.) The chloride contours mapped by the MCWRA (2017) for the 180-Foot Aquifer and the 400-Foot Aquifer are shown in Figure 1 with an orange line and a red line, respectively. Water quality information from privately owned wells is offered to MCWRA, but the locations of those wells are not released to the public. Available to us were the locations of the dedicated monitoring wells operated by government agencies that were used as control points for the creation of the 500 mg/L chloride contours from 2017. These wells account for approximately 63% of the wells used as control points in creating the chloride contours shown in Figure 1 (A. Woodrow, personal communication, 2019). These two aquifers have historically been used to support the highly productive local agriculture industry as well as to supply municipal water. The extent of saltwater intrusion — beyond 10 km inland in the 180-Foot Aquifer — as well as the continued inland advance of saltwater in both aquifers has stimulated groundwater management efforts to prevent further intrusion into these aquifers. These groundwater management efforts require a thorough understanding of the current distribution of salinity in each aquifer.

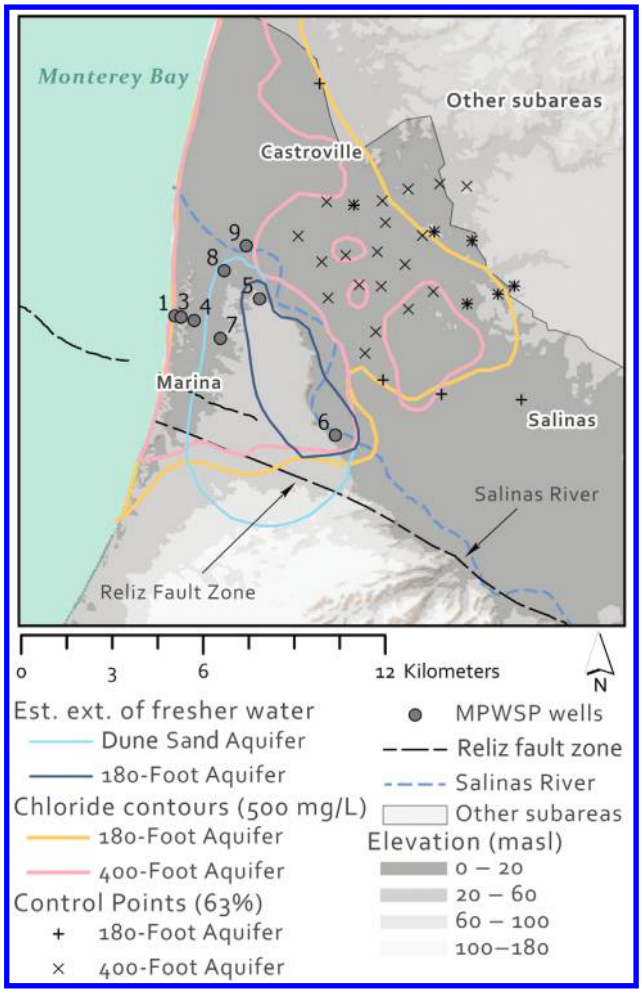

Figure 1. Map of the study area. Shown as the gray points are the eight monitoring wells for the MPWSP. Outlined in orange and red are the MCWRA contours, indicating a chloride content of 500 mg/L or greater, for the 180-Foot Aquifer and the 400-Foot Aquifer, respectively, as measured in 2017. Available control points used to create the chloride contours are shown as crosses. The location of the Salinas River is shown as a dashed blue line, whereas the location of the Reliz fault zone is shown as a dashed black line. Outlined in blue and dark blue are the estimated regions of low-salinity groundwater in the DSA and the 180-Foot Aquifer, respectively. Shaded in gray is the region including the subareas outside the 180/400-Foot Aquifer subarea.

Figure 2 shows a simplified schematic of the regional hydrostratigraphy as a cross section running roughly parallel to the coast. The unconfined aquifers, the Dune Sand Aquifer (DSA) in the south and the Perched "A" Aquifer (PAA) in the north, overlie the Salinas Valley Aquitard (SVA), which confines the flow of water into the underlying 180-Foot Aquifer. In turn, the 180-Foot Aquifer is separated from the underlying 400-Foot Aquifer by the 180/400-Foot Aquitard.

The current understanding of the hydrostratigraphy (Figure 2) and of the extent of saltwater intrusion (Figure 1) relies on information from wells. Although useful, well data are limited in spatial sampling and often do not provide sufficient detail to fully capture lateral variations in lithology and salinity. The vertical variation in salinity is also difficult to ascertain with water quality samples from a well because groundwater across the entire screened interval, which in wells in the study area can be as long as 200 m, are mixed within the well. These shortcomings in existing well data leave critical questions that need to be addressed to develop effective management plans to prevent ongoing saltwater intrusion. Two of these questions are addressed in this study.

The first question concerns the DSA and the 180-Foot Aquifer. Figure 1 shows the 180-Foot Aquifer to be intruded from the coast to a distance of up to 10 km inland. However, between 2014 and 2015, groundwater with concentrations of total dissolved solids (TDS) low enough to be classified as a source of drinking water (State Water Resources Control Board, 2006) was detected in the 180-Foot Aquifer in two of the eight monitoring well clusters (MW-5 and MW-6) recently constructed for the Monterey Peninsula Water Supply Project (MPWSP); these well clusters are shown in Figure 1 as the gray circles. This suggested the presence of a lens

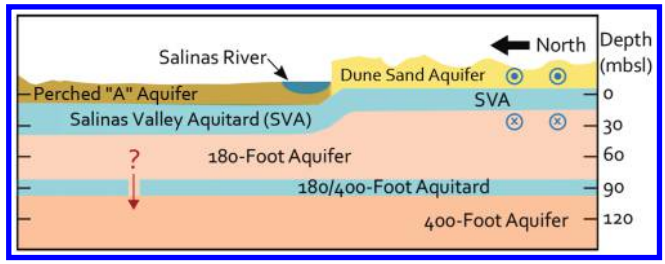

Figure 2. Simplified schematic of the hydrostratigraphy in the study area, showing the average elevations and thicknesses of each hydrostratigraphic unit. The Dune Sand Aquifer exists only south of the Salinas River. The circled dots and the underlying circled crosses in blue represent groundwater flowing in the Dune Sand Aquifer toward the coast (out of the image as dots), into the 180-Foot Aquifer, and then inland (into the image as crosses). The red arrow and question mark represent the vertical migration of saline groundwater from the 180-Foot Aquifer to the 400-Foot Aquifer.

DOI:10.1190/geo2019-0272.1

of fresher groundwater in this aquifer, outlined in Figure 1 in dark blue. Water of the same quality (a source of drinking water) also was detected in the overlying DSA in four of the eight MPWSP monitoring well clusters, which suggested the presence of a lens of fresher groundwater in this aquifer, outlined in Figure 1 in light blue. Saltwater was measured in the remaining three wells screened within the DSA (MW-1, MW-3, and MW-4), with progressively lower salinity with distance inland from the coast. Lithologic information has shown that the DSA and the 180-Foot Aquifer are hydraulically connected near the coast, and water level data have led to the conclusion that low-salinity groundwater in the DSA flows toward the coast and into the underlying 180-Foot Aquifer due to the differences in hydraulic head (MACTEC, 2005). This is shown schematically in Figure 2 as the circled dots and circled crosses in blue, which represent low-salinity groundwater flowing in the DSA toward the coast (out of the image as dots), downward into the 180-Foot Aquifer, and then inland (into the image as crosses). The current understanding is that fresher water flowing from the DSA into the 180-Foot Aquifer contributes to a natural hydraulic barrier that prevents saltwater intrusion in the 180-Foot Aquifer. For effective groundwater management of the 180-Foot Aquifer, the following question must be answered: what is the amount and distribution of this fresher groundwater in the DSA and the 180-Foot Aquifer? Given the water management objectives, the specific salinity level of interest is water with low enough salinity to be classified as a source of drinking water. Answering this question will help groundwater managers plan appropriate actions to prevent further saltwater intrusion into the 180-Foot Aquifer.

The second question involves the interaction between the 180-Foot Aquifer and the 400-Foot Aquifer. A report by Kennedy/Jenks Consultants (2004) note locations where the 180/400-Foot Aquitard was either thin or absent, and it predicted that saltwater in the 180-Foot Aquifer could migrate downward into the 400-Foot Aquifer. This vertical migration would have especially negative consequences in inland areas where the aquifer was unaffected by saltwater intrusion. For the first time in 2017, the MCWRA's map of saltwater intrusion displayed three isolated chloride contours in the 400-Foot Aquifer, inland of the previously mapped extent of saltwater intrusion; these areas are circled in red in Figure 1. Although this observation provides strong circumstantial evidence that saltwater is indeed flowing vertically from the 180-Foot Aquifer to the 400-Foot Aquifer, the extent of the region where saltwater is flowing between the aquifers may be underestimated because identifying this region would require high-quality lithologic logs and sufficient water quality information from each aquifer. Drilling and sampling wells for this purpose are time consuming and costly, and useful drilling locations are difficult to determine a priori. This leads to the question: What is the extent of saltwater that has reached the 400-Foot Aquifer from the 180-Foot Aquifer, as represented in Figure 2 with a red arrow and question mark? We intend to answer this question by finding locations where saltwater crosses from the 180-Foot Aquifer into the 400-Foot Aquifer.

In coastal regions, electrical geophysical methods — including electromagnetic and direct current resistivity methods — have been used to help image the distribution of salinity within coastal aquifers and complement data acquired within wells. These methods have proven effective due to the sharp contrast in electrical resistivity between fresh and saline water. For decades, ground-based methods have been used to identify regions containing freshwater and saltwater (van Dam and Meulenkamp, 1967; de Breuck and de Moor, 1969; Urish and Frohlich, 1990; Frohlich et al., 1994). More recent studies have continued to characterize the hydrostratigraphy and salinity of coastal regions (Martínez et al., 2009; Nenna et al., 2013; Martorana et al., 2014; Goebel et al., 2017), as well as to calibrate numerical saltwater intrusion models (Herckenrath et al., 2013) and inspect coastal hydrogeological features that can localize saltwater intrusion, such as paleochannels (Maillet et al., 2005). Resistivity structures estimated from these methods can be imaged from the ground surface to 20 m below ground surface (mbgs) for small-scale electrical resistivity tomography studies and to a maximum of 800 mbgs for audiomagnetotelluric methods (Nenna et al., 2013). Along the coast within the study region, Goebel et al. (2017) use an electrical resistivity tomography system to map out electrical resistivity to a depth of nearly 300 mbgs to investigate the distribution of fresh- and saltwater in the region. However, no electrical geophysical methods have been used on a large scale inland in the Monterey Bay area.

The AEM method used in our study has been used increasingly in applications to groundwater resources. This geophysical surveying method uses a time-domain electromagnetic system mounted on an aircraft, allowing for up to 400 line-km of data to be acquired in a day of surveying. Some of the challenges of using the AEM method in coastal environments include the presence of saltwater, the low resistivity of which quickly attenuates the electromagnetic signal. Frequency-domain airborne systems also have been used to investigate saltwater intrusion (Fitterman and Deszcz-Pan, 1998; Steuer et al., 2007; Delsman et al., 2018; Siemon et al., 2019). Although frequency-domain systems offer higher resolution in the near surface, they generally cannot image as deeply as time-domain systems because of the range of frequencies used. Thus, because of these higher frequencies, frequency-domain electromagnetic (FDEM) systems have had difficulties imaging below thick packages of conductive saltwater-saturated sediments (Siemon et al., 2009). In addition, FDEM systems transmit and receive a signal simultaneously, and, as a result, can have a lower signal-to-noise ratio (S/N). With the time-domain AEM method, there is a greater possibility of imaging below saltwater-saturated sediments.

In a few cases, the AEM method has been used to image the resistivity of aquifers impacted by seawater. On the west coast of Denmark, Kirkegaard et al. (2011) use AEM data to estimate the salinity of the Ringkøbing lagoon. Along the border of Germany and Denmark, Jørgensen et al. (2012) use an AEM system to identify preferential flow paths for the movement of seawater in the region. Teatini et al. (2011) use AEM data to map the extent of hydrostratigraphic units and the presence of freshwater beneath the Venice Lagoon. Using seismic and resistivity data, the authors identify gaps in a confining layer in the shallow subsurface that facilitate the movement of seawater across hydraulically conductive units. Pedersen et al. (2017) identify the presence of fresh and saline groundwater onshore and offshore using AEM data acquired near the coast of the Netherlands. Most recently, Goebel et al. (2019) acquire AEM data in the offshore region in the northern part of Monterey Bay, 20 km north of our study area. Each of these studies extracts valuable hydrologic information from AEM data acquired in coastal environments.

This study aims to improve the understanding of the distribution of freshwater and saltwater in the northern Salinas Valley by integrating the existing information with insights from recently acquired AEM data. Our specific objectives are (1) to obtain a high-quality resistivity model of the coastal aquifers in the northern Salinas Valley, (2) to transform this resistivity model to map out fresher water and saltwater in the study area, and (3) to answer the two pressing groundwater

management questions in the area. Through this case history, we add to the growing understanding of the ways in which the AEM method can be used to successfully address hydrogeologic questions in challenging coastal environments such as the northern Salinas Valley.

METHODS

Acquisition, processing, and inversion of AEM data

A total of 635 line-km (395 line-miles) of AEM data were acquired in the study area on 16–18 May 2017. We used a SkyTEM 304M time-domain electromagnetic system, which uses a helicopter to tow an electromagnetic transmitter and receiver. Cities and highways must be avoided during an AEM survey, leaving gaps in the flight lines. To acquire data, a strong current is applied to the transmitter coil to produce a magnetic field, after which the current in the transmitter coil is turned off to induce eddy currents in the subsurface. As these eddy currents decay, they induce secondary, time-varying magnetic fields, whose change in flux with time is measured in the receiver coil. The system continually cycles between use of a low-moment and a high-moment transmitter, which have peak moments of 3000 and 160,000 Am^2, respectively. Data are unusable at the beginning of the measurement period due to effects from the transmitter and at the end of the measurement period due to the diminishment of the signal below the noise floor. In this study, we were able to use data between 8.42 μs and 6.85 ms after the transmitter reached peak current. Details of the method and the SkyTEM system can be found in Sorensen and Auken (2004).

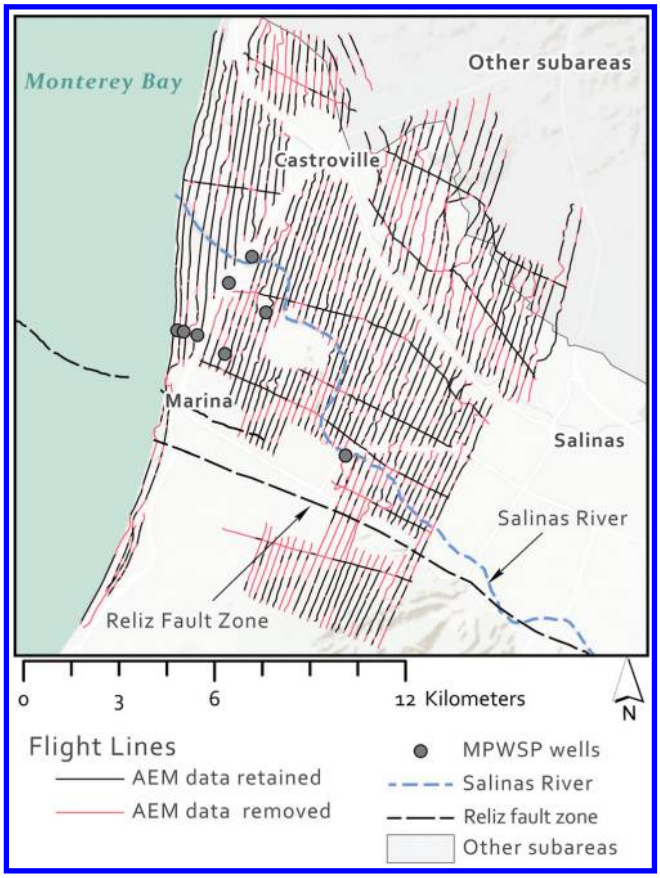

Figure 3. Flight lines of the AEM survey. Flight lines corresponding to where AEM data were retained for processing are shown as the black lines, whereas flight lines corresponding to where AEM data were removed during processing are shown as red lines. As in Figure 1, the locations of the MPWSP monitoring wells are shown as gray circles, the Salinas River is shown as a dashed blue line, and the location of the Reliz fault zone is shown as a dashed black line. Cities and highways were avoided during the AEM survey, leaving gaps in the flight lines.

The data collected in this survey were processed and inverted using the software package Aarhus Workbench. During processing, the raw data were stacked, and contaminated data were identified manually and removed. The primary sources of data contamination in AEM surveys in developed regions, such as the study area, are coupling with objects such as powerlines, fences, and buried cables or pipes (Danielsen et al., 2003), as well as noise from the signal transmitted by the powerlines. The flight lines for the AEM survey, which are, with a few exceptions, spaced 200–300 m apart, are shown in Figure 3. The flight lines for the AEM survey are shown in Figure 3. The flight lines corresponding to the data retained during processing correspond to 61.3% of all of the acquired data and are shown in black. This relatively low percentage of retained data is due to the high number of powerlines, pipelines, and other infrastructure that was encountered during this AEM survey. The retained, high-quality data were inverted using a laterally constrained inversion (Auken and Christiansen, 2004), which constrains estimated resistivity values to the values estimated from nearby data collected along a single flight line. The inverted resistivity model has 30 layers, each with a fixed depth, increasing logarithmically in thickness from 3 m at the surface to 24 m at 280 mbgs. The logarithm of resistivity values in the same layer at adjacent soundings is constrained to be within a factor of 1.6 of each other, whereas the logarithm of resistivity values vertically adjacent to each other is constrained to be within a factor of 2.7 within the first 100 m; beyond 100 m, this factor increases according to a power law. The altitude was also a parameter in the inversion, with the recorded value during the survey input as an initial value and an uncertainty of 1.3 m ascribed to the measurement. Resistivity values obtained from the AEM data span a wide range, exceeding 500 ohm-m in regions above the top of the saturated zone south of the Salinas River, and falling below 1 ohm-m near the coast.

The depth of investigation (DOI) is used as an approximate measure to indicate the depth above which the resistivity estimates made from AEM data are reliable. The DOI was estimated at every location where data were inverted using the method described by Christiansen and Auken (2012). The DOI is a sensitivity-based measure used to indicate the depth below which resistivity values tend to be less well resolved. The DOI varies significantly across the study region due to a dependence on the resistivity structure, as well as noise levels and the signal strength. We found it to be approximately 50 mbgs in the more conductive regions along the coast and generally 150–200 mbgs in the more resistive inland regions.

Transforming the resistivity model

Although processing and inversion of AEM data yield a high-resolution model of the subsurface resistivity, what is needed to interpret the locations of fresher water and saltwater is a transform from resistivity to a measure of salinity. Although measurement of the electrical resistivity of the water alone can be a direct water salinity indicator, the electrical resistivity of a volume of subsurface material is determined not just by the water salinity, but also by the texture and mineralogy of the sediments and the volume of water

DOI:10.1190/geo2019-0272.1

present. This means that clay-rich sediment, in addition to saltwater, can decrease the resistivity values. A summary of the controls on the electrical resistivity of geologic materials is given by Knight and Endres (2005). In our study region, the lithology of the subsurface is documented as being highly heterogeneous, where aquifer units contain numerous silt and clay lenses from fluvial, alluvial, and marine deposits. An additional complicating factor is the presence of the unsaturated zone near the ground surface, where resistivity values typically increase significantly and abruptly due to a reduction in the volume of water for electrical conduction.

To obtain information about salinity from the AEM data, we first identified the top of the saturated zone (TSZ). Water table measurements were available contemporaneous with the collection of AEM data in the eight MPWSP monitoring well clusters in the study area (see Figure 1). Each cluster is comprised of three wells, one of which is screened within the unconfined aquifer. We used these measurements as an approximation of the TSZ, assuming the capillary rise in the relatively coarse dune sands would be negligible in comparison to the vertical resolution of the AEM resistivity model, which is at best 3 m. Aside from the measurements in the MPWSP wells contemporaneous with the AEM survey, few water table measurements exist in the hilly dune deposits south of the Salinas River because most wells in the region are not screened in the unconfined DSA. Therefore, we used the resistivity model derived from the AEM data to assist in estimating the elevation of the TSZ. We did this by defining a resistivity cutoff to be used to separate the unsaturated zone from the saturated zone in the AEM resistivity model. All resistivity values greater than the cutoff corresponded to the unsaturated zone; those less than the cutoff corresponded to the saturated zone, with the interface between the two regions corresponding to the TSZ. We optimized, through trial and error, the choice of the cutoff, finding that a resistivity cutoff of 75 ohm-m resulted in a good agreement between the elevation of the AEM-determined water table and the elevation of the water table based on the measurements in the eight MPWSP wells.

To answer the posed questions related to groundwater management in this area, we needed to relate the AEM resistivity values to salinity within the saturated zone. To do so, we used induction-based resistivity logging measurements acquired by others, recorded every 15 cm in seven of the eight MPWSP wells (MW-3 lacks a geophysical log), along with laboratory TDS measurements taken from each of the three screened intervals of each MPWSP well cluster. Each TDS measurement was assumed to be the salinity of the pore water contained in the sediments, although the measurement represents an average of the TDS across the screened interval. The water quality samples were taken approximately one to two months after drilling; wells were bailed before taking a water quality sample.

In Figure 4, we show the histogram of all of the resistivity logging measurements from the seven MPWSP wells, color coded to correspond to the measured TDS values, divided into three ranges of TDS concentration, based on public drinking water standards: TDS $\leq$ 3000 mg/L corresponds to a source of drinking water (State Water Resources Control Board, 2006), which we will refer to in this paper as fresher water, 3000 < TDS < 10,000 mg/L corresponds to water of potential beneficial use (U.S. Environmental Protection Agency, 1988), and TDS $\geq$ 10,000 mg/L corresponds to water of limited beneficial use (U.S. Environmental Protection Agency, 1988), which we will refer to as saltwater.

As shown in the data in Figure 4, there is an overlap in resistivity values for sediments saturated with water of TDS concentrations in the range 3000 < TDS < 10,000 mg/L and in the range TDS $\leq$ 3000 mg/L. However, we can define resistivity cutoffs to identify regions of the subsurface with groundwater with TDS $\leq$ 3000 mg/L (i.e., fresher water) and TDS $\geq$ 10,000 mg/L (i.e., saltwater), indicated in Figure 4 by blue bars and red bars, respectively. The resistivity cutoffs defined correspond to the background colors in Figure 4. We estimated that the resistivity of sediments saturated with saltwater is less than or equal to 3 ohm-m, and the resistivity of sediments saturated with fresher water falls between 20 and 75 ohm-m. We note that the resistivity cutoff of 75 ohm-m used to map the water table agrees well with the data shown in Figure 4, where the maximum resistivity value is 74 ohm-m. We do not explicitly account for the effect of clay on resistivity values and have no way to do so, given the available data. We instead use cutoffs that are based on resistivity values associated with all lithologies, including clay-rich sediment.

A group of borehole resistivity logging measurements with values between 20 and 30 ohm-m were obtained for sediments containing groundwater with concentrations in the range 3000 < TDS < 10,000 mg/L, shown in Figure 4 as the yellow bars with red outlines. These resistivity measurements are considered to be outliers, and they were not used when determining the resistivity cutoffs to identify sediments saturated with fresher water. Each of the measurements outlined in red in Figure 4 comes from resistivity logging measurements within the shallow screened interval of MW-9. Within this interval, a baseline TDS concentration of 3204 mg/L was measured, which places the measurement narrowly into the middle TDS range. The borehole resistivity was measured between 20 and 30 ohm-m within the sandy unit at the bottom of the screened interval (between 23 and 35 mbgs). Above this sandy interval, from approximately 20 to 23 mbgs, the borehole resistivity measurements drop, indicating that the water quality may have changed along with the recorded lithologic change to a more silt-rich sediment. The resistivity measurements from the nearest AEM measurements, 272 m away, also reflect this drop in resistivity. There-

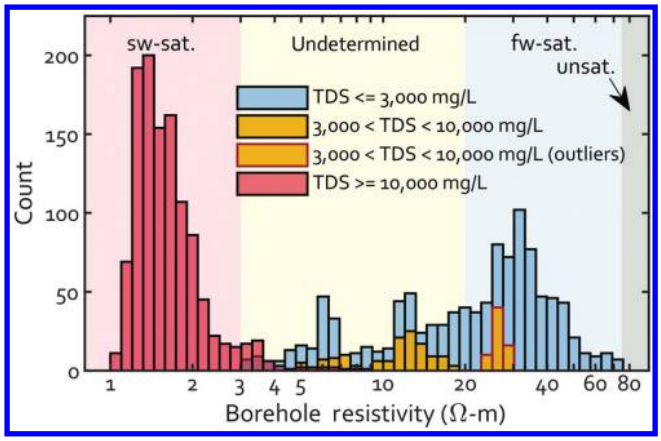

Figure 4. Values from resistivity logging measurements in the MPWSP monitoring wells, colored according to the defined TDS cutoffs. The bars colored purple between 3 and 4 ohm-m indicate an overlap of blue bars (TDS $\leq$ 3,000 mg/L) and red bars (TDS $\geq$ 10,000 mg/L). The background colors indicate the resistivity cutoffs defined to identify saltwater-saturated sediment ($\leq$3 ohm-m in red; "sw-sat."), sediment saturated with fresher water (20–75 ohm-m in blue; "fw-sat."), and unsaturated sediment ($\geq$75 ohm-m in gray; "unsat.").

fore, we conclude that the shallow screen of MW-9 likely spans intervals saturated with water of very different TDS concentrations, so that the baseline measurement of 3204 mg/L represents a mixing of water with those different TDS concentrations. For this reason, the baseline TDS measurement is not considered representative of the screened interval, and the resistivity measurements corresponding to this interval were not included when the resistivity cutoffs were chosen.

Because of our conservative approach to defining the cutoffs, we expect to underestimate the volume of sediments saturated with saltwater and the volume of sediments saturated with fresher water. This is especially true for sediments saturated with fresher water, where Figure 4 shows 41.5% of the resistivity values in this range overlap resistivity measurements from the other two TDS ranges. A summary of the defined resistivity cutoffs is given in Table 1.

Table 1. Summary of the defined ranges of resistivity values for saturated sediments and the corresponding ranges of TDS concentrations. The specific resistivity values chosen as cutoffs were based on the TDS measurements and resistivity measurements made in the MPWSP wells.

Description of salinity	TDS range	Resistivity of saturated sediments
Fresher water (source of drinking water)	≤3000 mg/L	20 – 75 ohm-m
Water of potential beneficial use	3000–10,000 mg/L	Undefined
Saltwater (water of limited beneficial use)	≥10,000 mg/L	≤3 ohm-m

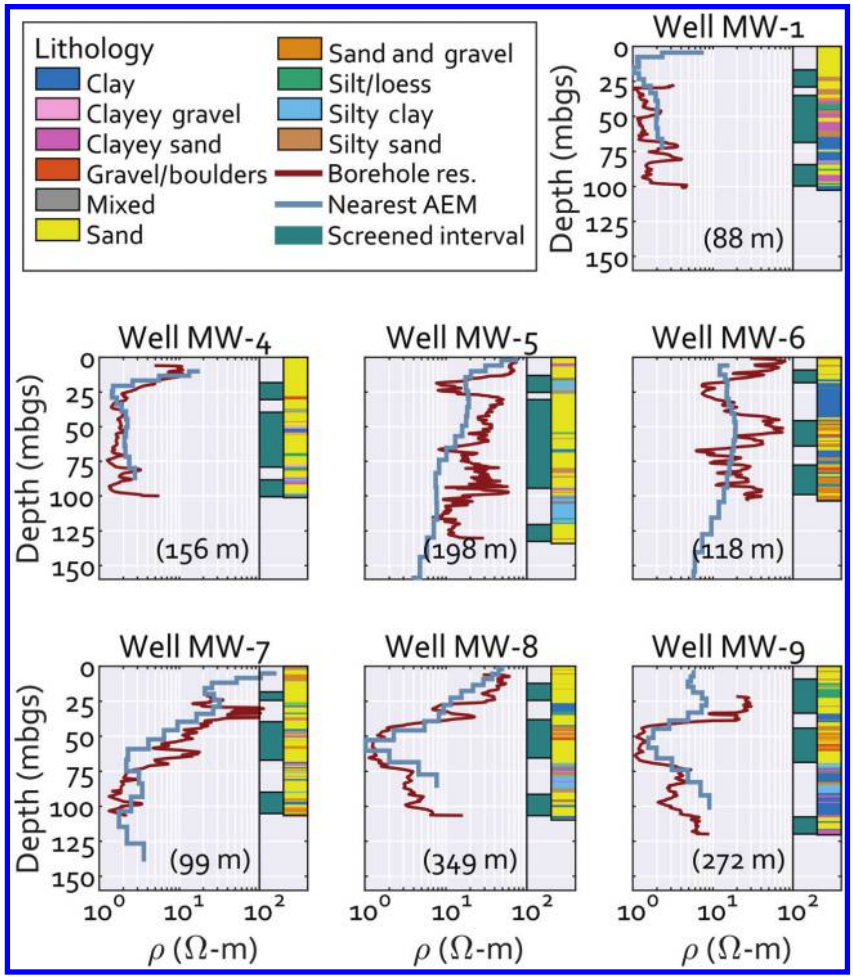

Figure 5. Comparison between borehole resistivity measurements in the MPWSP wells, shown as a red line, with the closest AEM resistivity measurements as a blue line. The distance between the location of each borehole resistivity log and the corresponding AEM resistivity measurements is shown in the bottom-right corner of each figure, in parentheses. The screened intervals of each MPWSP well cluster are shown in teal, and the lithology descriptions are shown on the far right.

RESULTS

Comparison of borehole and AEM resistivity values

To validate the acquired AEM data and the categories defined in Table 1, we compared the AEM resistivity estimates with borehole resistivity logging measurements from the study area. To make this comparison, the groundwater conditions at the time of the borehole measurements should reflect those present during the time of the AEM survey. The aquifers of the northern Salinas Valley experience dynamic changes in electrical resistivity due to the movement of fresher and saline water from active saltwater intrusion, tidal pumping, and annual recharge. For this study, we relied on measurements made in the existing MPWSP wells, which were logged approximately two years before the acquisition of AEM data. We compared the borehole resistivity logs from seven MPWSP wells with the AEM-derived resistivity estimates that were located closest to the wells.

Figure 5 shows the comparison between these sets of measurement for each of the seven MPWSP wells with borehole resistivity logs. The MPWSP borehole resistivity measurements are shown as a red line, along with the nearest AEM measurements in blue. The distance from each well to the nearest AEM measurements is shown in the bottom-right corner of each figure; from well to well, this distance ranges between 88 and 349 m. On the right side of each figure in teal boxes are shown the screened intervals of the MPWSP well cluster. Each screened interval represents a separate well in the MPWSP well cluster. On the far right side of each figure, the lithology descriptions are shown. The depth interval in Figure 5 is shown as depth from the ground surface at the location of the MPWSP monitoring well. To accommodate differences in the ground surface elevation between the MPWSP monitoring well and the nearest AEM measurements, the blue line is shifted according to the difference in elevation between the two points.

DOI:10.1190/geo2019-0272.1

Generally, there is very good agreement between the AEM estimates and the borehole measurements. The best agreement can be observed in monitoring wells MW-4, MW-7, and MW-8. The disparity is greatest between the borehole resistivity measurements in MW-6 and the nearest AEM resistivity estimates. The trend of the borehole geophysical measurements is captured between 70 and 100 mbgs; however, the fine-scale fluctuations in, and the magnitude of, borehole resistivity measurements are not fully captured in the AEM data in this case. We attribute the cause of the mismatch between the AEM and borehole resistivity measurements in this location to a lack of low-moment data and high noise levels in the acquired data near MW-6. Directly next to the Salinas River, there is an approximately 40 m gain in ground surface elevation, causing the helicopter to quickly change altitude and speed, thus swinging the transmitter and decreasing the S/N. In addition, there are powerlines near MW-6, which introduced significant noise into the low-moment AEM data in this area.

AEM resistivity model

We developed a hydrostratigraphic model of the study area using information from previously published reports (Harding ESE, 2001; Hanson et al., 2002; Kennedy/Jenks Consultants, 2004; MACTEC, 2005), updated with information from the AEM resistivity model and well data. This allows us to view horizontal slices through the resistivity model and interpret them in the context of the regional hydrostratigraphy. Figure 6 shows four maps of resistivity values in 10 m thick horizontal slices corresponding roughly to the elevations of four major hydrostratigraphic units. Resistivity values were averaged vertically across the 10 m thick slice, and they then were interpolated horizontally to produce a spatially continuous map. A radial basis function was used to interpolate the resistivity values, in which the highest weight was given to the closest lateral measurements and values of greater than 450 m away were not used. In each figure, the AEM flight lines are shown as thin black lines. Below the color scale for resistivity measurements (at the bottom of Figure 6) are indicated the defined ranges of resistivity values used to identify subsurface regions: the region ≤ 3 ohm-m corresponds to saltwater-saturated sediments ("ss"), the region between 20 and 75 ohm-m corresponds to sediments saturated with fresher water ("fs"), and the region ≥ 75 ohm-m corresponds to unsaturated sediments ("us"). Using this classification in Figure 6, we generally will refer to locations as containing fresher water or saltwater, instead of as having high or low resistivity.

Figure 6a shows the average resistivity values in the depth range between 5 and 15 mbsl, corresponding roughly to the PAA north of the Salinas River, to the DSA between the Salinas River and Reliz fault zone near the coast, and to the SVA between the Salinas River and the Reliz fault zone farther inland. The region along the coast in both aquifers is predictably saturated with saltwater due to saltwater intrusion. Just inland south of the Salinas River, we see regions of fresher water, which continue to a distance of approximately 8 km from the coast. Intermediate resistivity values are observed north of the Salinas River that are not low enough to be classified as saltwater and not high enough to be classified as fresher water. Patches of fresher water appear in the north, in and near the area marked "other subareas." This area represents a transition zone between the fluvial sediments of the Salinas Valley and the alluvial sediments of the Gabilan Range and has not been intruded by saltwater. South of the Reliz fault zone are two patches of very low resistivity; these same patches appear in Figure 6b–6d, and it may reflect buried structures in the area.

Figure 6b shows the average resistivity values in the depth range between 20 and 30 mbsl, which, south of the Salinas River, corresponds roughly to the top of the 180-Foot Aquifer, whereas north of the Salinas River corresponds roughly to the SVA. As in Figure 6a, the region along the coast is saturated with saltwater, representing the extent of saltwater intrusion at this elevation. Just inland, a large region containing fresher water is present south of the Salinas River, as shown in Figure 6a. North of the Salinas River, the average resistivity is lower than south of the river, as would be expected given the presence of the clay-rich (low resistivity) SVA. The resistivity values are higher than in the same region of Figure 6a, perhaps because the SVA has not been as affected by the more saline water in the overlying Perched "A," described in a report by Harding ESE (2001) as "highly mineralized water." As in Figure 6a, patches of fresher water appear in and near the area marked other subareas.

Figure 6c shows the average resistivity values in the depth range between 50 and 60 mbsl, corresponding roughly to the 180-Foot Aquifer. The chloride contour (orange) indicates the landward extent of saltwater intrusion in the 180-Foot Aquifer. The AEM resistivity values indicate saltwater in the sediments along the coast and extending inland. The inland boundary to the region identified, with the AEM data, as being saltwater-saturated approximately parallels the chloride contour, but it does not reach as far inland. A likely explanation for this difference in location is the definition of "saltwater," where we define saltwater as TDS values greater than 10,000 mg/L, and the MCWRA draws its line at the 500 mg/L chloride contour. Based on chemical analysis of groundwater in the area, chloride accounts for approximately 55% of the TDS concentration in the California Central Coast (Geoscience Support Services, 2014). For reference, this means that 10,000 mg/L TDS is approximately 5500 mg/L chloride, a concentration of just more than 10 times higher than that of the MCWRA chloride contours. Assuming that in California the TDS of the ocean is approximately 33,000 mg/L, the MCWRA chloride contours represent approximately 3% salinity and the 10,000 mg/L, and TDS value represents approximately 30% salinity.

Figure 6d shows the average resistivity values in the depth range between 100 and 110 mbsl, corresponding roughly to the 400-Foot Aquifer. Unlike Figure 6a–6c, there are regions in the study area where no resistivity values are shown because they are below the DOI. The chloride contour (red) indicates the landward extent of saltwater intrusion in the 400-Foot Aquifer. In addition, there are some isolated regions farther inland mapped by MCWRA. Much of the region along the coast is below the DOI due to the low-resistivity saltwater in the overlying section. Where resistivity data are available along the coast, we see regions containing saltwater and larger regions of saltwater-saturated sediments farther inland. As above, the boundary outlining the saltwater-saturated region roughly parallels, but does not reach as far inland as, the chloride contour.

North of the Salinas River, many small regions of lower resistivity (in some cases, low enough to be classified as saltwater) can be observed. As will be shown in a cross section, many of these are continuous vertical features, extending from the base of the overlying 180-Foot Aquifer down to the DOI, suggesting that they are associated with the downward migration of saltwater from the 180-Foot Aquifer.

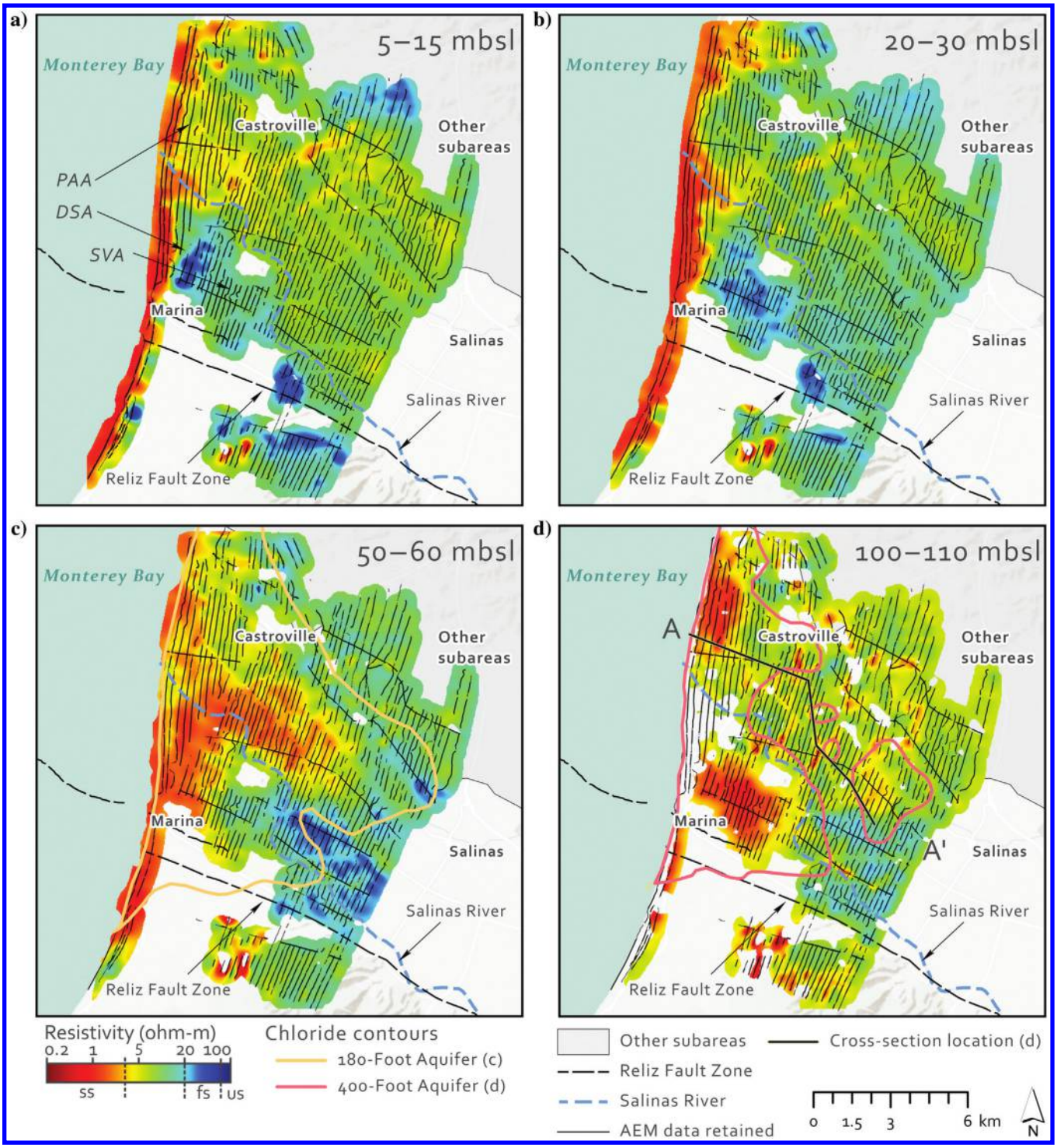

Figure 6. Images of interpolated values of average resistivity (a) between 5 and 15 mbsl, corresponding roughly to the unconfined aquifers in the region, (b) between 20 and 30 mbsl, corresponding roughly to the Salinas Valley Aquitard north of the Salinas River, (c) between 50 and 60 mbsl, corresponding roughly to the 180-Foot Aquifer, and (d) between 100 and 110 mbsl, corresponding roughly to the top of the 400-Foot Aquifer. In each figure, the Salinas River is shown as a dashed blue line and the Reliz fault zone as a dashed black line. The aquifers roughly corresponding to the elevation in Figure 6a (5–15 mbsl) are annotated: the PAA north of the Salinas River, the DSA between the Salinas River and Reliz fault zone near the coast, and to the SVA between the Salinas River and the Reliz fault zone farther inland. The chloride contour for the 180-Foot Aquifer is shown in orange in Figure 8c, and the 400-Foot chloride contours are shown in Figure 8d in red. Also shown in Figure 8d is the location of the cross section A-A′, which will be used for further analysis.

DOI:10.1190/geo2019-0272.1

Mapping fresher water in the DSA and the 180-Foot Aquifer

Let us now consider our first question: what is the amount and distribution of groundwater in the DSA and the 180-Foot Aquifer with low enough salinity to be classified as a source of drinking water? This has been defined as water with a concentration of TDS $\leq$ 3000 mg/L and is referred to in this study as fresher water. We have classified the AEM resistivity values between 20 and 75 ohm-m as corresponding to sediments saturated with fresher water. Using the hydrostratigraphic model of the study area that we developed, we can assign the presence of fresher water to either the DSA or the 180-Foot Aquifer.

Figure 7a displays the interpreted thickness saturated with fresher water of the DSA; we have included the surficial dunes along the coast as part of the DSA. We note that the very thick surficial aquifer south of the Reliz fault zone is undifferentiated from the DSA and has been grouped with the DSA in Figure 7a, but is not necessarily composed of dune sand deposits. The colors of the thickness map range from light blue to dark blue, representing a range from 0 to 170 m. The DSA only exists south of the Salinas River, increasing in thickness from roughly 30 m in most of the study area to approximately 130 m south of the Reliz fault zone. The locations of AEM data retained for processing are shown as black lines, and the Salinas River is shown here in brown. The area encircled in red is the estimated extent, based on well data, of the DSA containing fresher water (shown in Figure 1 as a light-blue line).

With a few exceptions, everywhere the AEM data were acquired, we interpret the DSA to contain fresher water, with the thickness of fresher water ranging from approximately 15% to 75% of the total thickness of the aquifer. Here, we are using the boundaries from our developed hydrostratigraphic model to determine the thickness of the DSA at any given point. Estimates of 3.6–9.7 m for the fresher water-saturated thickness of the aquifer, derived from well measurements, were made in Marina in 2001 (MACTEC, 2005). These measurements were taken as part of a monitoring program using a dense network of wells, albeit over a relatively small region restricted to Marina, with the nearest wells in the network always separated by fewer than 500 m. As can be seen in Figure 7a, interpretation of the AEM resistivity data indicates that the thickness of the DSA containing fresher water is generally between 5 and 15 m north of the Reliz fault zone, slightly higher than the estimates based on 2001 water table measurements in wells. In some cases, this thickness interpreted from AEM data is greater than 25 m, although this is generally not the case. The most likely cause for this discrepancy is the difference in precipitation between the two years (2016/17 was an especially wet winter, whereas 2000/01 was relatively normal). However, other factors may affect this discrepancy, including the vertical discretization of the AEM resistivity model (the smallest layer thickness of which is 3 m) and the ability of the AEM system

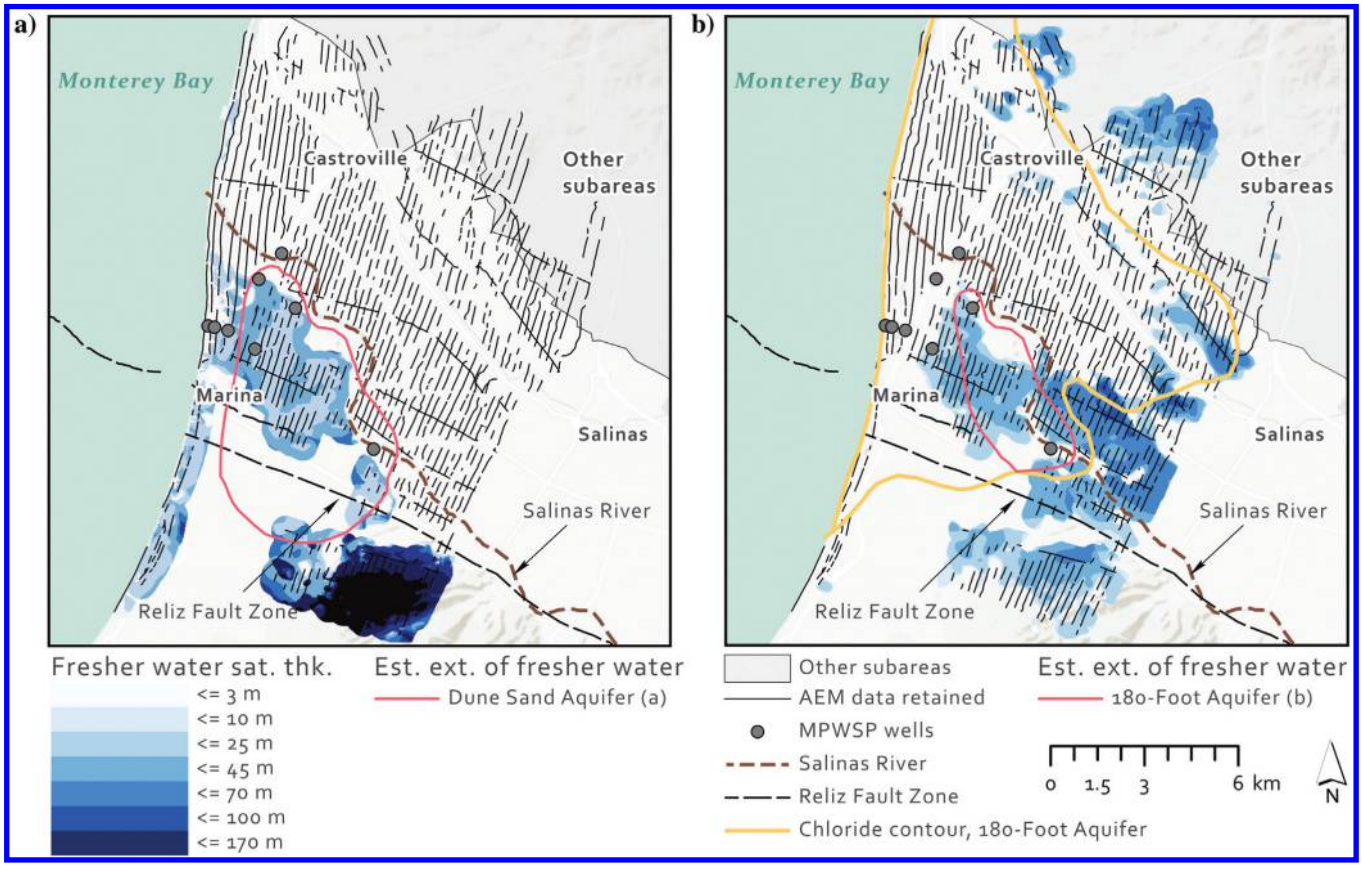

Figure 7. Interpreted thickness of the (a) Dune Sand Aquifer saturated with freshwater and (b) the 180-Foot Aquifer saturated with freshwater. Both thickness plots are shown in a color scale ranging from light to dark blue. In each figure, the extent of freshwater estimated using well data is shown for the corresponding aquifer and is outlined in red. The locations where AEM data were collected and retained for processing are shown as black lines. The Salinas River is shown as a dashed brown line.

to accurately resolve the boundaries of the aquifer. The estimate of the fresher water-saturated thickness of the aquifer derived from AEM measurements also may differ from the estimate using well measurements due to the fact that the former detect the TSZ while the wells measure the depth to the water table. Moving from north to south of the Reliz fault zone, the thickness of sediments saturated with fresher water grows dramatically, ranging from 10 to 150 m, according to AEM resistivity data. This corresponds to the thickening of the DSA in this region.

The thickness of the 180-Foot Aquifer saturated with fresher water is shown in Figure 7b. For reference, the 180-Foot Aquifer thickens from approximately 50 m throughout most of the study area to approximately 120 m in the area marked other subareas in the north. Again, the AEM lines are shown in black, the Salinas River is shown in brown, and the color scheme ranges from light blue to dark blue, displaying the thickness of the aquifer saturated with fresher water. The area circled in red is the estimated extent, based on well data, of the 180-Foot Aquifer containing freshwater (shown in Figure 1 as a dark-blue line). The MCWRA chloride contour for the 180-Foot Aquifer is shown as an orange line. South of the Salinas River, the AEM data reveal fresher water extending from about one kilometer from the coast throughout the entire region where AEM data are collected; i.e., there is a significant amount of fresher water falling within the area mapped as saltwater by the MCWRA chloride contour. North of the Salinas River, the interpretation of the AEM data is in good agreement of the MCWRA chloride contour, with little fresher water seen seaward of the contour. There is no fresher water interpreted in the 180-Foot Aquifer along the Salinas River near MW-6. As previously discussed, the AEM resistivity estimates near MW-6 are expected to be affected by high noise levels and removed data points. The resulting values of the resistivity estimates are near 10 ohm-m (as shown in Figure 5), which is near the center of the range of "undetermined" resistivity values. In other words, these data remain uninterpreted and do not enter into our thickness estimation of fresher water-saturated and saltwater-saturated sediment. At the northern extent of the study area, in and near the area marked other subareas in Figure 7b, is a

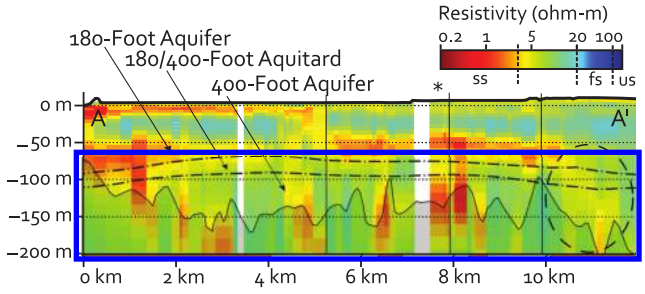

Figure 8. Cross section of the AEM resistivity model along the cross section, the location of which is shown in Figure 6d. The region below the depth of investigation is shaded in gray. Dashed lines indicate the approximate boundary of the 180/400-Foot Aquitard. The red line underneath the cross section marks the region inside the MCWRA chloride contour for the 400-Foot Aquifer. The three vertical black lines on the cross section (near 5, 8, and 10 km) indicate the locations where the direction of the cross section changes. The asterisk above the cross section near 8 km indicates where we analyzed the uncertainty in the 1D resistivity model. The circled area past 10 km indicates where saltwater is interpreted as migration of saltwater from the 180-Foot Aquifer to the 400-Foot Aquifer, despite that the resistivity values are higher than 3 ohm-m.

transition zone between the fluvial deposits of the Salinas Valley and the alluvial fan deposits of the area marked other subareas to the north. Due to active recharge in this upland area, saltwater is not expected to intrude far inland. This is what is seen in the MCWRA chloride contour and in the locations of fresher water mapped by the AEM data.

Mapping locations of vertical saltwater migration

We now address our second question: what is the extent of saltwater that has reached the 400-Foot Aquifer from the 180-Foot Aquifer? We have classified the AEM resistivity values fewer than 3 ohm-m as corresponding to saltwater-saturated sediments, and we now locate regions where the 180-Foot Aquifer and the 400-Foot Aquifer contain saltwater.

The horizontal slice of resistivity data corresponding to the 400-Foot Aquifer, shown in Figure 6d, shows isolated regions containing saltwater mapped by the AEM system north of the Salinas River. The most logical explanation for these features is the downward migration of saltwater from the 180-Foot Aquifer into the 400-Foot Aquifer, which MCWRA similarly suggests is the explanation for isolated chloride contours in the 400-Foot Aquifer (MCWRA, 2017). Saltwater rising from the aquifer below the 400-Foot Aquifer is a possible but unlikely explanation for the presence of isolated saltwater in the 400-Foot Aquifer. The 400-Foot Aquifer is separated from the aquifer below by a marine clay layer up to 100 m thick (Kennedy/Jenks Consultants, 2004); there is little evidence of saltwater in this underlying aquifer inland of the coastal area. Some low-resistivity features also appear in the transition zone from fluvial sediment to alluvial fan sediment in and around the region marked other subareas in Figure 6d; however, we do not have sufficient salinity and borehole resistivity data from this region to build a transform from resistivity to salinity, so we focus our interpretation on the rest of the study area.

In Figure 8, we show a vertical cross section, the location of which is indicated in Figure 6d as A-A′, through the AEM resistivity model beginning near the coast and extending inland, intersecting each of the closed chloride contours, which indicate isolated regions of saltwater. The AEM resistivity values are projected onto the cross section from up to 120 m away to reduce gaps in the cross section. The dashed lines in Figure 8 correspond to the approximate boundary of the 180/400-Foot Aquitard, as indicated by the developed hydrostratigraphic model. As can be seen from left to right in Figure 8, the AEM resistivity model indicates that saltwater is present in the 180-Foot Aquifer and the 400-Foot Aquifer. Although the presence of saltwater is mostly continuous in the 180-Foot Aquifer up to 10 km inland, saltwater appears discontinuously in the 400-Foot Aquifer, above and below the DOI; the region shaded in gray in Figure 8 signifies the region below the DOI. The part of the cross section up to the 4 km mark corresponds to the study area inside the primary chloride contour for the 400-Foot Aquifer, shown as a red bar underlying the cross section in Figure 8. The presence of saltwater observed in the AEM data in this area is very likely the result of saltwater intrusion from the coast. The isolated regions of saltwater, seen inland of this in the AEM data for the 400-Foot Aquifer, are likely the result the vertical migration of saltwater from the overlying 180-Foot Aquifer because saltwater is present above these locations in the 180-Foot Aquifer. Two regions where saltwater is present inland in the 400-Foot Aquifer, near 6.5 km and between 7.5 and 8.2 km, correspond closely to the locations of

DOI:10.1190/geo2019-0272.1

the isolated, closed chloride contours for the 400-Foot Aquifer, shown as the red bars underlying the cross section in Figure 8. The region between 7.5 and 8.2 km is larger than is indicated by the chloride contour. We suspect that this difference is due to better spatial sampling with the AEM data than with the well-based MCWRA data set. Closer to the coast, at approximately 5 km, another region containing saltwater is mapped by the AEM data but is not captured by the chloride contours; again, this could be due to the limited spatial sampling in the MCWRA data set.

Just beyond 10 km along the cross section, the low resistivity values indicating saltwater in the 180-Foot Aquifer increase to approximately 5 ohm-m (a yellow color), and this spans the 180-Foot Aquifer, the 180/400-Foot Aquitard, and the 400-Foot Aquifer. This location, which is circled in Figure 8, corresponds very well to the region inside the easternmost MCWRA chloride contour, shown under the cross section in Figure 8 as a red bar. Although the resistivity values are slightly higher than our resistivity cutoff of 3 ohm-m for saltwater-saturated sediments, this was a conservative cutoff value, and the continuity of the feature across the 180/400-Foot Aquitard boundary supports the interpretation of this being indicative of the downward migration of the saltwater.

The AEM data from the northern Salinas Valley also raise the possibility of saltwater migrating vertically from the PAA to the underlying 180-Foot Aquifer. Approximately 5 km along the cross section shown in Figure 8, the low resistivity values indicating saltwater in the PAA span the SVA and the 180-Foot Aquifer, suggesting that saltwater may be flowing through a thin or absent portion of the SVA; in contrast, throughout most of Figure 8, the SVA is characterized by a resistivity of approximately 10 ohm-m between 10 and 40 mbgs. Although a very few well-based data exist for the PAA, data from one well, approximately 7.5 km inland, show that groundwater levels in the PAA at the location of the well have been below sea level for decades. Water levels below sea level in an unconfined aquifer connected to the sea may indicate that groundwater is flowing to another aquifer where water levels are lower — in the case of the northern Salinas Valley, this may be the 180-Foot Aquifer. The groundwater flow in this area warrants further investigation because a hydraulic connection between the PAA and the 180-Foot Aquifer could impact existing efforts to mitigate intrusion of saltwater into the 180-Foot Aquifer.

DISCUSSION

Hydrogeologic relevance of fresher water in the DSA and the 180-Foot Aquifer

The acquired AEM data augment the understanding of the spatial distribution of, and connection between, fresher water in the DSA and the 180-Foot Aquifer. The extent of fresher water in both aquifers has been interpreted to extend farther toward the coast and farther south than was interpreted using the MPWSP well data. Given the interpreted continuity of fresher water through most of the DSA and the 180-Foot Aquifer south of the Salinas River, it is reasonable to assume that fresher water extends beyond the locations where AEM data were acquired; however, this should be verified with water quality measurements.

The acquired AEM data help reveal the amount and distribution of fresher water in the DSA available to flow into the 180-Foot Aquifer near the coast. The resulting groundwater mound in the 180-Foot Aquifer also creates the conditions for passive-active saltwater intrusion (Werner, 2017), where the groundwater gradient points toward the sea on the seaward side of the mound and inland on the landward side of the mound. The increased head of the groundwater mound acts as a hydraulic barrier to saltwater intrusion, although it is important to note that saltwater with sufficiently high pressure still will be able to migrate beneath the mound of fresher water and continue inland. Passive-active saltwater intrusion in the coastal Salinas Valley has been described by previous hydrogeologic reports in the area (MACTEC, 2005). Here, some of the fresher water entering the 180-Foot Aquifer from the DSA flows seaward and presumably exits to the ocean as submarine groundwater discharge. However, the hydraulic gradient within the 180-Foot Aquifer east of the mound points landward, indicating that some of this fresher water entering the 180-Foot Aquifer flows inland. The substantial lens of fresher water-saturated sediment in the 180-Foot Aquifer south of the Salinas River, which we interpret from the AEM data to be up to 37 m thick, is evidence of this process.

Imaging saltwater-saturated sediments at depth

Inland in the study area, we have interpreted the deep, low-resistivity features in the AEM resistivity model as horizontally isolated saltwater in the 400-Foot Aquifer. The continuous vertical sampling of the AEM data offers a more complete picture of the vertical distribution of saltwater than can be obtained by water quality sampling from wells, which typically are screened over depth intervals ranging between 20 and 100 m. However, there are challenges when using AEM systems to image deep, saltwater-saturated sediments. The generally conductive subsurface in coastal regions attenuates the AEM signal quickly, resulting in a shallow DOI, whereas the small difference in resistivity between the background resistivity (often between 5 and 10 ohm-m) and the target resistivity (here $\leq$3 ohm-m) makes imaging the isolated regions of saltwater more difficult than they were in a resistive background. Furthermore, regions of isolated saltwater-saturated sediments are not laterally continuous, calling into question the 1D assumption that was made in this study, and that is commonly made, when inverting AEM data. To have confidence in the interpretation of the deep, low-resistivity features in the AEM resistivity model, we needed to better understand the uncertainty in the resistivity model.

We analyzed the uncertainty in the 1D resistivity model at a location where we interpreted the presence of a low-resistivity zone in the 400-Foot Aquifer; this location is marked with an asterisk in Figure 8. This was done by inverting the corresponding AEM data using a Markov chain Monte Carlo (MCMC) approach. The 1D resistivity model, which had been obtained from using a laterally constrained inversion (LCI), is shown in Figure 9 as a blue line. We inverted for a five-layer resistivity model, selecting as a starting model the one shown in Figure 9, which is a good approximation of the 1D resistivity model. The low-resistivity feature in the 400-Foot Aquifer is in the fourth layer centered at 150 mbgs. We inverted for the resistivity and thickness of each model layer, as well as the altitude of the transmitter used in the acquisition of the AEM data. We used a uniform distribution for the step size between model iterations and ran 10,000 model iterations.

The results of the MCMC inversion are shown in Figure 10 as a matrix of plots, displaying the estimated distribution of the resistivity ρ, depth d, and thickness t of the fourth layer, the layer of interest, in the five-layer model. Along the diagonal of the matrix is a

DOI:10.1190/geo2019-0272.1

normalized, smoothed histogram for the estimated value of each parameter, with a black vertical line indicating the maximum value. The three plots in the upper right corner are scatter plots of the sampled values from the inversion between pairs of parameters. Each of the three plots in the lower left corner shows a density contour of the sampled values, where dark blue indicates a high density of the values sampled in each iteration. The uppermost histogram in Figure 10 shows that the resistivity of the fourth layer in the five-layer model is constrained to lie between approximately 2 and 3 ohm-m, meaning that in almost all iterations the fourth layer would be classified as saltwater-saturated sediments by our resistivity cutoff. The depth and thickness of the layer are both constrained to a range of approximately 20 m, as can be seen in the middle and lower histograms, respectively. The depth range, between approximately 120 and 140 m, corresponds to the 400-Foot Aquifer. The results of this inversion demonstrate that the deep, low-resistivity feature is reproduced consistently with the dimensions and at the depth that we would expect. Thus, despite the challenges of imaging in this coastal environment, we are confident in our interpretation of the low-resistivity features in the 400-Foot Aquifer.

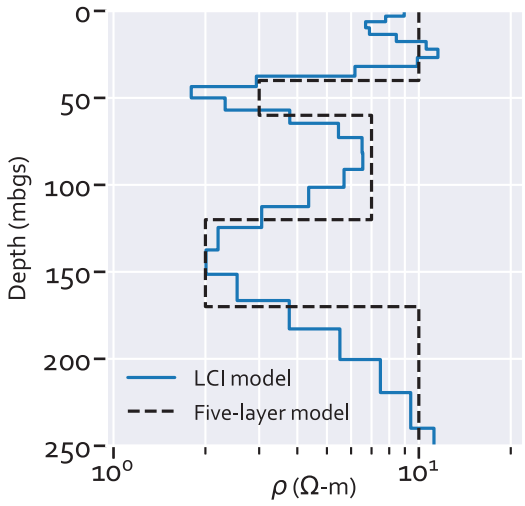

Figure 9. AEM resistivity model from acquired data (LCI model) shown in blue, along with a five-layer model, shown as a dashed black line, used as the starting model in the MCMC inversion. Of particular interest is the uncertainty of the fourth layer because this layer is interpreted to represent isolated saltwater in the 400-Foot Aquifer.

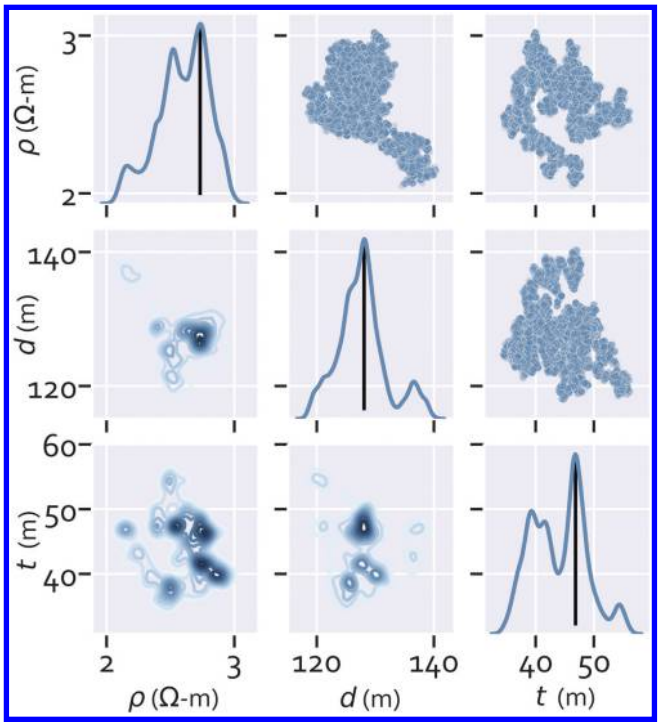

Figure 10. Matrix of plots showing the distribution of the resistivity ρ, depth d, and thickness t of the fourth layer from the MCMC inversion. The plots on the diagonal show a smoothed, normalized histogram of parameter values. The plots in the upper right corner are scatterplots of pairs of sampled parameter values, whereas the plots in the lower left corner show the density of the sampled parameter values.

CONCLUSION

The AEM data acquired within the northern Salinas Valley in May 2017 have provided a model of the electrical resistivity of the subsurface, offering insights into the locations of fresher water and saltwater in the study area. After processing and inversion, the AEM data were used to estimate the electrical resistivity of the subsurface from the ground surface to, generally, between 50 and 200 mbgs. Using TDS measurements and resistivity logging measurements within wells, resistivity cutoffs were defined, corresponding to saltwater-saturated sediments (TDS $\geq$ 10,000 mg/L) and sediments saturated with fresher water (TDS $\leq$ 3000 mg/L), which then were applied to the AEM resistivity data.

The use of the AEM method in this coastal area allowed us to address the two key questions relevant for local groundwater management. Locations containing fresher water were mapped across the DSA and the 180-Foot Aquifer in the study area, and isolated saltwater was mapped in the 400-Foot Aquifer. The results of the study provided several insights into the regional hydrogeology. In the DSA and in the 180-Foot Aquifer, the AEM resistivity measurements show that fresher water extends farther toward the coast and farther south than had been interpreted previously using well data. Furthermore, isolated bodies of saltwater were imaged successfully in the 400-Foot Aquifer from the AEM resistivity data, supporting the suggestion that saltwater is migrating downward from the 180-Foot Aquifer to the 400-Foot Aquifer in certain locations. For this method to reliably map out fresher water and saltwater in heterogenous aquifers, sufficient high-quality lithology, salinity, and borehole resistivity data were needed. Applying the defined resistivity threshold map regions of fresher water and saltwater was effective across the study region. However, manual interpretation still was needed in some locations where the resistivity data did not fall into the defined categories.

The acquired AEM data provide an excellent view into the complex pattern of salinity within the northern Salinas Valley, expanding the set of data currently available for managing the groundwater resources in the region. This case study demonstrates that the AEM method can be applied successfully to map out fresher water and saltwater in a challenging coastal environment such as the northern Salinas Valley.

ACKNOWLEDGMENTS

Funding for this project was provided by the Marina Coast Water District. Additional funding to Stanford University was provided by the Zeitgeist Foundation and the S. D. Bechtel Jr. Foundation. We thank Seequent for providing the Leapfrog Geo software and Keith Van Der Maaten, Curtis Hopkins, Jesse Crews, and Ahmad Behroozmand for their contributions and helpful discussions. We thank two anonymous reviewers whose thoughtful comments helped to improve the quality of this manuscript.

DATA AND MATERIALS AVAILABILITY

Data associated with this research are available and can be obtained by contacting the corresponding author.

REFERENCES

Auken, E., and A. V. Christiansen, 2004, Layered and laterally constrained 2D inversion of resistivity data: Geophysics, **69**, 752–761, doi: 10.1190/1.1759461.

Breuck, W. de, and G. de Moor, 1969, The water-table aquifer in the Easter Coastal Area of Belgium: Bulletin of the International Association of Scientific Hydrology, **14**, 137–155, doi: 10.1080/02626666909493739.

Christiansen, A. V., and E. Auken, 2012, A global measure for depth of investigation: Geophysics, **77**, no. 4, WB171–WB177, doi: 10.1190/geo2011-0393.1.

Dam, J. C. van, and J. J. Meulenkamp, 1967, Some results of the geo-electrical resistivity method in groundwater investigations in The Netherlands: Geophysical Prospecting, **15**, 92–115, doi: 10.1111/j.1365-2478.1967.tb01775.x.

Danielsen, J. E., E. Auken, F. Jørgensen, V. Søndergaard, and K. I. Sørensen, 2003, The application of the transient electromagnetic method in hydrogeophysical surveys: Journal of Applied Geophysics, **53**, 181–198, doi: 10.1016/j.jappgeo.2003.08.004.

Delsman, J. R., E. S. van Baaren, B. Siemon, W. Dabekaussen, M. C. Karaoulis, P. S. Pauw, T. Vermaas, H. Bootsma, P. G. de Louw, J. L. Gunnink, and C. W. Dubelaar, 2018, Large-scale, probabilistic salinity mapping using airborne electromagnetics for groundwater management in Zeeland, the Netherlands: Environmental Research Letters, **13**, 084011, doi: 10.1088/1748-9326/aad19e.

Fitterman, D. V., and M. Deszcz-Pan, 1998, Helicopter EM mapping of saltwater intrusion in everglades National Park, Florida: Exploration Geophysics, **29**, 240–243, doi: 10.1071/EG998240.

Frohlich, R. K., D. W. Urish, J. Fuller, and M. O'Reilly, 1994, Use of geoelectrical methods in groundwater pollution surveys in a coastal environment: Journal of Applied Geophysics, **32**, 139–154, doi: 10.1016/0926-9851(94)90016-7.

Geoscience Support Services, 2014, Monterey Peninsula Water Supply Project Hydrogeologic Investigation: Summary of Results — Exploratory Boreholes: Prepared for California American Water and RBF Consulting, https://bc5dd67e-5897-4c4b-b2f6-a34fa14a3caf.filesusr.com/ugd/28b094_77e1c04f67224f67a5703fa0443c6751.pdf, accessed 14 May 2020.

Goebel, M., R. Knight, and M. Halkjær, 2019, Mapping saltwater intrusion with an airborne electromagnetic method in the offshore coastal environment, Monterey Bay, California: Journal of Hydrology: Regional Studies, **23**, 100602, doi: 10.1016/j.ejrh.2019.100602.

Goebel, M., A. Pidlisecky, and R. Knight, 2017, Resistivity imaging reveals complex pattern of saltwater intrusion along Monterey Coast: Journal of Hydrology, **551**, 746–755, doi: 10.1016/j.jhydrol.2017.02.037.

Hanson, R. T., R. R. Everett, M. W. Newhouse, S. M. Crawford, M. I. Pimentel, and G. A. Smith, 2002, Geohydrology of deep-aquifer system monitoring-well site at Marina, Monterey County, California: U.S. Geological Survey Water-Resources Investigations Report 02–4003, http://pubs.water.usgs.gov/wri024003, accessed 14 May 2020.

Harding ESE, 2001, Hydrogeologic investigation of the salinas valley basin in the vicinity of Fort Ord and Marina, Salinas Valley, California: Prepared for Monterey County Water Resources Agency, https://www.co.monterey.ca.us/home/showdocument?id=19570, accessed 14 May 2020.

Herckenrath, D., G. Fiandaca, E. Auken, and P. Bauer-Gottwein, 2013, Sequential and joint hydrogeophysical inversion using a field-scale groundwater model with ERT and TDEM data: Hydrology and Earth System Sciences, **17**, 4043–4060, doi: 10.5194/hess-17-4043-2013.

Jørgensen, F., W. Scheer, S. Thomsen, T. O. Sonnenborg, K. Hinsby, H. Wiederhold, C. Schamper, T. Burschil, B. Roth, R. Kirsch, and E. Auken, 2012, Transboundary geophysical mapping of geological elements and salinity distribution critical for the assessment of future sea water intrusion in response to sea level rise: Hydrology and Earth System Sciences, **16**, 1845–1862, doi: 10.5194/hess-16-1845-2012.

Kennedy/Jenks Consultants, 2004, Hydrostratigraphic Analysis of the Northern Salinas Valley: Prepared for Monterey County Water Resources Agency, https://www.co.monterey.ca.us/home/showdocument?id=19582, accessed 14 May 2020.

Kirkegaard, C., T. O. Sonnenborg, E. Auken, and F. Jørgensen, 2011, Salinity distribution in heterogeneous coastal aquifers mapped by airborne electromagnetics: Vadose Zone Journal, **10**, 125–135, doi: 10.2136/vzj2010.0038.

Knight, R., and A. Endres, 2005, An introduction to rock physics principles for near-surface geophysics: Near Surface Geophysics, **1**, 31–70, doi: 10.1190/1.9781560801719.ch3.

MACTEC, 2005, Operable unit carbon tetrachloride plume groundwater remedial investigation / feasibility study, former Fort Ord, California: Prepared for The U.S. Army Corps of Engineers, http://www.fortordcleanup.com/ar_pdfs/AR-OUCTP-0011P/Volume_I_RI/VolumeIFinalRItext.pdf.

Maillet, G. M., E. Rizzo, A. Revil, and C. Vella, 2005, High resolution electrical resistivity tomography (ERT) in a transition zone environment: Application for detailed internal architecture and infilling processes study of a Rhône River Paleo-Channel: Marine Geophysical Researches, **26**, 317–328, doi: 10.1007/s11001-005-3726-5.

Martínez, J., J. Benavente, J. L. García-Aróstegui, M. C. Hidalgo, and J. Rey, 2009, Contribution of electrical resistivity tomography to the study of detrital aquifers affected by seawater intrusion-extrusion effects: The River Vélez Delta (Vélez-Málaga, Southern Spain): Engineering Geology, **108**, 161–168, doi: 10.1016/j.enggeo.2009.07.004.

Martorana, R., L. Lombardo, N. Messina, and D. Luzio, 2014, Integrated geophysical survey for 3D modelling of a coastal aquifer polluted by seawater: Near Surface Geophysics, **12**, 45–59, doi: 10.3997/1873-0604.2013006.

Monterey County Water Resources Agency, 2017, Recommendations to address the expansion of seawater intrusion in the Salinas Valley Groundwater Basin, https://www.co.monterey.ca.us/home/showdocument?id=57396, accessed 14 May 2020.

Nenna, V., D. Herckenrath, R. Knight, N. Odlum, and D. Mcphee, 2013, Application and evaluation of electromagnetic methods for imaging saltwater intrusion in coastal aquifers?: Seaside Groundwater Basin, California: Geophysics, **78**, no. 2, B77–B88, doi: 10.1190/geo2012-0004.1.

Pedersen, J. B., F. W. Schaars, A. V Christiansen, and N. Foged, 2017, Mapping the fresh-saltwater interface in the coastal zone using high-resolution airborne electromagnetics: First Break, **35**, 57–61.

Siemon, B., A. V. Christiansen, and E. Auken, 2009, A review of helicopter-borne electromagnetic methods for groundwater exploration: Near Surface Geophysics, **7**, 629–646, doi: 10.3997/1873-0604.2009043.

Siemon, B., E. van Baaren, W. Dabekaussen, J. Delsman, W. Dubelaar, M. Karaoulis, and A. Steuer, 2019, Automatic identification of fresh-saline groundwater interfaces from airborne electromagnetic data in Zeeland, the Netherlands: Near Surface Geophysics, **17**, 3–25, doi: 10.1002/nsg.12028.

Sorensen, K. I., and E. Auken, 2004, SkyTEM — A new high-resolution helicopter transient electromagnetic system: Exploration Geophysics, **35**, 194–202, doi: 10.1071/EG04194.

State Water Resources Control Board, 2006, Adoption of Policy Entitled "Sources of Drinking Water" Resolution No. 88–63, https://www.waterboards.ca.gov/board_decisions/adopted_orders/resolutions/2015/rs2015_0002.pdf, accessed 14 May 2020.

Steuer, A., B. Siemon, and D. Eberle, 2007, Airborne and Ground-Based Electromagnetic Investigation of the Freshwater Potential in Tsunami-Hit Areas of Northern Sumatra: Proceedings of the Symposium on the Application of Geophysics to Engineering and Environmental Problems, SAGEEP, **1**, 265–275.

Teatini, P., L. Tosi, A. Viezzoli, L. Baradello, M. Zecchin, and S. Silvestri, 2011, Understanding the hydrogeology of the Venice lagoon subsurface with airborne electromagnetics: Journal of Hydrology, **411**, 342–354, doi: 10.1016/j.jhydrol.2011.10.017.

Urish, D. W., and R. K. Frohlich, 1990, Surface electrical resistivity in coastal groundwater exploration: Geoexploration, **26**, 267–289, doi: 10.1016/0016-7142(90)90008-G.

U.S. Environmental Protection Agency, 1988, Guidelines for Ground-Water Classification Under the EPA Ground-Water Protection Strategy, https://nepis.epa.gov/Exe/ZyPURL.cgi?Dockey=9100L950.TXT, accessed 14 May 2020.

Werner, A. D., 2017, On the classification of seawater intrusion: Journal of Hydrology, **551**, 619–631, doi: 10.1016/j.jhydrol.2016.12.012.